ISBN: 978-3-95450-184-7 doi:10.18429/JACoW-IPAC2018-THPAK061

MAGNETIZED AND FLAT BEAM GENERATION AT THE FERMILAB'S FAST FACILITY*

A. Halavanau[1,2], P. Piot[1,2], D. Edstrom Jr.[1], A. Romanov[1],
D. Crawford[1], J. Ruan[1], D. Mihalcea[1], V. Shiltsev[1] , S. Nagaitsev[1]
[1] Fermi National Accelerator Laboratory, Batavia IL 60510, USA
[2] Department of Physics and Northern Illinois Center for Accelerator & Detector Development, Northern Illinois University DeKalb, IL 60115, USA

Abstract

Canonical-angular-momentum (CAM) dominated beams can be formed in photoinjectors by applying an axial magnetic field on the photocathode surface. Such a beam possess asymmetric eigenemittances and is characterized by the measure of its magnetization. CAM removal with a set of skew-quadrupole magnets maps the beam eigenemittances to the conventional emittances along each transverse degree of freedom, thereby yielding a flat beam with asymmetric transverse emittance. In this paper, we report on the experimental generation of CAM dominated beam and their subsequent transformation into flat beams at the Fermilab Accelerator Science and Technology (FAST) facility. Our results are compared with numerical simulations and possible applications of the produced beams are discussed.

INTRODUCTION

Magnetized and flat beam generation was proposed by Derbenev [1] and pioneered at Fermilab's A0 facility [2–4]. Recently, these beams were produced at FAST facility [5]. In brief, when electrons are born in the presense of a strong axial magnetic field, they form an electron beam with prevalent angular motion. The measure of this motion is known as Canonical Angular Momentum (CAM) and is given by [6, 7]:

$$L = \gamma m r^2 \dot{\theta} + \frac{1}{2} e B_z(z) r^2 + O(r^4). \quad (1)$$

Such beams could be decoupled in a rount-to-flat beam (RTFB) adapter to form a beam with asymmetric transverse emittances or a flat beam. The latter type beams have various interesting applications in dielectric laser acceleration and plasma wakefield acceleration. Additionally, they can serve as probes for nonlinearities in accelerating cavities. One can show the new eigenemittances associated to CAM are [1, 8–11]:

$$\epsilon_\pm = \sqrt{\epsilon_{4D}^2 + \mathcal{L}^2} \pm \mathcal{L} \rightarrow \epsilon_+ \approx 2\mathcal{L}; \epsilon_- \approx \frac{\epsilon_{4D}^2}{2\mathcal{L}}, \quad (2)$$

where ϵ_{4D} is the uncorrelated 4D emittance and $\mathcal{L} = L/2p_z$ Magnetized beam production at FAST facility was theoretically considered in [12].

* This work is supported by the DOE contract No.DEAC02-07CH11359 to the Fermi Research Alliance LLC. The work of A.H. is supported by the US Department of Energy under contract No. DE-SC0011831 with Northern Illinois University.

FAST FACILITY

FAST is a superconducting 300 MeV electron linac currently under commissioning at Fermilab [5, 13]. FAST includes a ~ 50-MeV photoinjector. The RF gun solenoids were designed to provide strong axial magnetic field at the photocathode surface thereby generating CAM dominated or magnetized beams. Hereafter we consider the experimental beamline described in [5] with the nominal beam parameters provided by Table 1 and the beamline elements detailed in Table 2.

Table 1: Low-Energy Beamline Parameters of the IOTA/FAST Injector

Parameter	Value	Units
Transverse emittance (norm.)	<1	μm
Beam energy	50	MeV
Slice energy spread	<5	keV
Nominal charge	250	pC
Bunch duration	5	ps

Table 2: FAST low-energy beamline key components and their locations. Skew-quadrupoles are denoted in italic font.

Quadrupoles	Pos. (m)	**YAG screens**	Pos. (m)
Q106	8.682	X107	8.905
Q107	8.883	X111	10.540
Q108	9.491	X121	17.420
Q109	9.873	**Cavities**	-
Q110	10.255	CC1	4.030
Q111	10.459	CC2	5.500
Q112	11.004	**Slits**	-
Q113	11.205	X107	8.905
Q120	16.285	X118	15.900

During the FAST Run-2017, CAM beams were produced using bucking solenoid as a source of the axial magnetic field. The main solenoid was used to match initial beam Twiss parameters into the round-to-flat beam (RTFB) adapter. The magnetic field at the cathode as a function of solenoids' currents is plotted in color in Fig. 1. The maximum values of currents were limited by the corresponding beam dynamics downstream of the RF gun.

MAGNETIZATION MEASUREMENTS

The CAM-dominated 34 MeV electron beam was formed with a laser distribution depicted in Fig. 2. The value of

ISBN: 978-3-95450-184-7 doi:10.18429/JACoW-IPAC2018-THPAK061

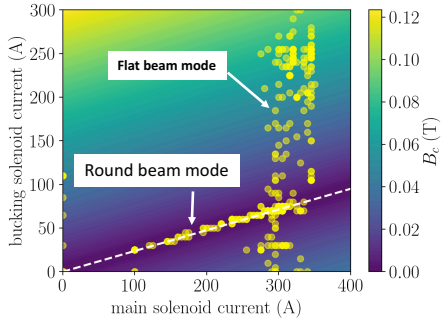

Figure 1: Axial magnetic field at the photocathode as a function of bucking and main solenoid currents at FAST.

CAM was measured with both multi-slit and quadrupole scan methods and the results are in a good mutual agreement. The magnetic field was reconstructed using the map shown in Fig. 1.

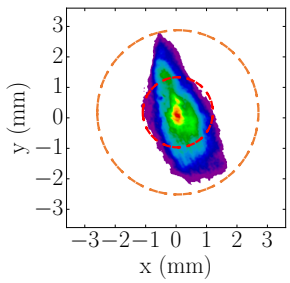

Figure 2: Initial asymmetric FAST photocathode laser distribution. The RMS sizes of orange and red circles are 950 µm and 520 µm respectively.

In order to measure the value of CAM provided to the electron beam we inserted horizontal multi-slits at X107 location and observed the beamlet rotation downstream of the slits using a YAG screen located at the X111 diagnostics station. The measured rotation angle between the mask and the beamlets images at the X111 provides a measurement of the beam's CAM L which can be deduced from [2]:

$$L = 2p_z \frac{\sigma_1 \sigma_2 \sin\theta}{D}, \tag{3}$$

where $\sigma_{1,2}$ are the measured beam sizes at the multi-slit mask and the screen location respectively, $D = 1.6$ m is the drift length between the mask and the screen. We refer the reader to Refs. [2, 3] for a detailed description of the method. In order to perform the calculation, the beam sizes at both locations have to be registered. Then the multi-slit mask is inserted and the tilt angle θ is determined. The measurement process is demonstrated in Fig. 3 for different bucking solenoid currents. In the bucked configuration, the horizontal multi-slits at the X107 location are seen to be horizontal downstream at the X111 screen. With the increase of the bucking solenoid current, the residual axial magnetic field at the photocathode increases, imposing the angular momentum on the beam. Latter results in the beamlets

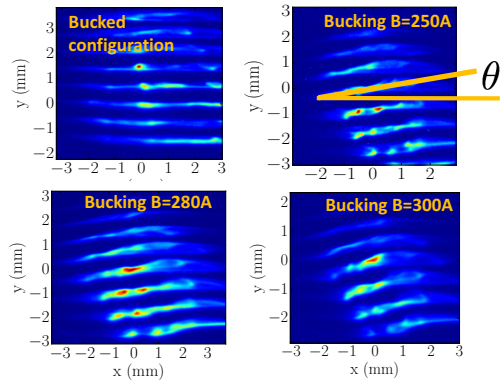

Figure 3: CAM value measurement using multi-slit mask at X107 location for different configurations of the FAST RF-gun solenoids.

rotation, as depicted in Fig. 3. Additionally, the slits method

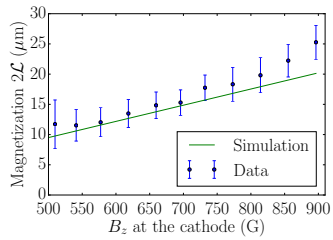

Figure 4: Measured CAM as a function of the cathode surface magnetic field $B_{0z} \equiv B_z(0)$ compared with IMPACT-T simulations.

can be extended to the case of multi-beam array discussed in [14].

One can show that transformation of the magnetized beam covariance matrix Σ_0 in the quadrupole

$$\Sigma_1 = \mathbf{R_{drift}}\mathbf{R_{quad}}\Sigma_0(\mathbf{R_{drift}}\mathbf{R_{quad}})^T$$

yields to the equation for MAM

$$L = \langle xy \rangle / d^2 q, \tag{4}$$

where q is the quadrupole strength and d is the drift length. Thus, electron beam magnetization can be inferred from a quadrupole scan by fitting values of $< xy >$ for different settings of q. Note, that in practice the calculation of the resulting moment $< xy >$ in case of a small L can be altered by finite resolution of the beam viewer setup. In that case, one can substitute quadrupole with a skew quadrupole, and the resulting equation for MAM is

$$L = |\langle x^2 \rangle - \langle y^2 \rangle| / 2d^2 q. \tag{5}$$

The results are shown in Fig. 5 and found to be in a good agreement with numerical simulations. For the flat beam

ISBN: 978-3-95450-184-7 doi:10.18429/JACoW-IPAC2018-THPAK061

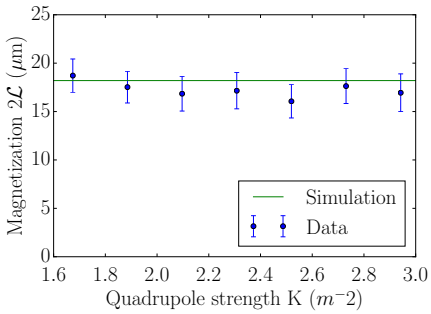

Figure 5: Measured CAM generated by B_z = 734 Gauss using quadrupole scan method and comparison with IMPACT-T simulations.

generation experiment, we selected the bucking solenoid current of 255 A, which ensured stable machine operation while maintaining acceptable vacuum levels in the RF gun. This corresponds to the maximum residual axial magnetic field applied on the cathode of 734 G. Both techniques were proved to be reliable and fast for the CAM measurement and can be extended to the higher values of CAM in different experimental conditions.

FLAT BEAM GENERATION

CAM can be removed from the electron distribution via round-to-flat beam (RTFB) transformation. A typical RTFB adapter consists of 3 skew-quadrupoles with its strengths specified by [12]:

$$q_1 = \pm\sqrt{\frac{-d_2(d_T s_{21} + s_{11}) + d_T s_{22} + s_{12}}{d_2 d_T s_{12}}},$$
$$q_2 = \frac{(d_2 + d_3)(q_1 - s_{21}) - s_{11}}{d_3(d_2 q_1 s_{11} - 1)}, \quad (6)$$
$$q_3 = \frac{d_2(q_2 - q_1 q_2 s_{12}) - s_{22}}{d_2(d_3 q_2 s_{22} + q_1 s_{12} - 1) + d_3(s_{12}(q_1 + q_2) - 1)},$$

where d_2, d_3 are the distances between first and second, and second and third quadrupole respectively, $d_T = d_2 + d_3$, s_{ij} are the elements of 2×2 matrix S that is defined in [8]. Note, that the solutions given by Eq. (6) will be identical for both orange and red circles in Fig. 2 and won't depend on the value of L.

In order to investigate the mapping of the eigenemittances defined by Eq. (2) due to CAM, we first performed a numerical simulation of the RTFB transformation in IMPACT-T [15]. We converted a laser distribution at FAST photocathode into a macroparticle distribution similarly to [14]. As displayed in Fig. 2 the initial laser distribution is asymmetric, therefore the axisymmetric flat beam solution given by Eq. (6) has to be refined. In case of a low beam charge (Q=20 pC), the three thick-lens RTFB adapter model was numerically optimized with the conjugate-gradient method using MAGNETOPTIMIZER [16]. The optimized quadrupole currents were

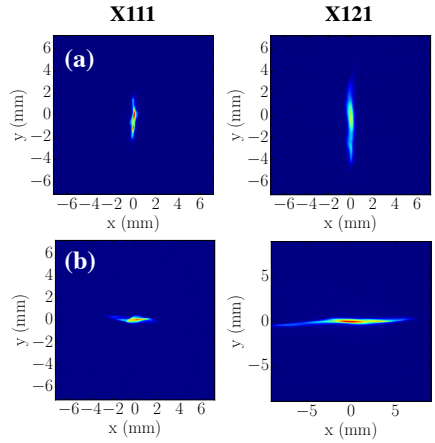

Figure 6: Measured optimized vertical and horizontal flat beams produced from the beam with CAM due to the residual magnetic field of 734 Gauss at the photocathode.

then dialed back into the machine and the CAM removal process recorded at X111 location.

The final emittance measurement after the RTFB adapter optimization was performed using a quadrupole scan technique. The resulting flat beam normalized emittances generated from the beam with CAM of approximately L = 18 µm were measured to be: ϵ_x = 0.13 µm, ϵ_y = 14.4 μm for the vertical flat beam and ϵ_x = 0.17 µm, ϵ_y = 12.7 µm for the horizontal flat beam. The beam images for the aforementioned cases appear in Fig. 6 and the associated emittance measurements are summarized in Table 3.

Table 3: Comparison of measured emittances for the cases of vertical and horizontal round-to-flat beam transformation compared with numerical simulations in IMPACT-T.

Experimental results			
Norm. emit.	Vert. fb	Hor. fb	Units
ϵ_x	0.13 ± 0.03	12.7 ± 2.79	µm
ϵ_y	14.4 ± 3.17	0.17 ± 0.04	µm
ϵ_{4D}	1.37 ± 0.42	1.47 ± 0.49	µm
IMPACT-T simulations			
ϵ_x	0.08	17.7	µm
ϵ_y	18.0	0.10	µm
ϵ_{4D}	1.20	1.33	µm

CONCLUSIONS

We obtained both horizontal and vertical flat beams and the measured emittances are in a decent agreement with the numerical simulations of the RTFB transform. We experimentally demonstrated the flat beam generation from a non-round laser spot at the photocathode. The discrepancy between the simulations and measurement is partially attributed to the limitation of quadrupole scan technique, e.g. measuring extremely low emittances requires longer baselines and significant optics adjustments. Flat beams will be used in the future FAST experiments.

ISBN: 978-3-95450-184-7 doi:10.18429/JACoW-IPAC2018-THPAK061

REFERENCES

[1] Ya. Derbenev. Adapting optics for high-energy electron cooling, UM-HE-98-04-A, (1998).

[2] Y. E Sun, P. Piot, K. J. Kim, N. Barov, S. Lidia, J. Santucci, R. Tikhoplav, and J. Wennerberg. *Phys. Rev. ST Accel. Beams*, **7**, 123501 (2004).

[3] Y. Sun, "Angular-momentum-dominated electron beams and flat-beam generation", Ph.D. Dissertation, University of Chicago, Chicago, USA (2005).

[4] Y. E Sun, P. Piot, K. J. Kim, *Phys. Rev. ST Accel. Beams*, **9**, 031001 (2006).

[5] S. Antipov, *et al*, *Journal of Instrumentation*, 12(03):T03002, (2017).

[6] H. Busch, *Annalen der Physik*, **386**, 974–993, (1926).

[7] M. Reiser. *Theory and design of charged particle beams* (1995).

[8] K. J. Kim. *Phys. Rev. ST Accel. Beams*, 6:104002, (2003).

[9] R. Brinkmann, Ya. Derbenev, and K. Flottmann. *Phys. Rev. ST Accel. Beams*, **4**, 053501 (2001).

[10] S. Nagaitsev and A. Shemyakin, FERMILAB-TM-2107, (2000).

[11] S. Lidia. *LUX Tech Note-012, LBNL-56558* (2012).

[12] A. Halavanau, P. Piot, *et al*, *FERMILAB-CONF-17-172-APC*, (2017).

[13] A. Romanov, *et al*, *Proc. of IPAC2018*, Vancouver, Canada, paper THPMF024, (2018).

[14] A. Halavanau *et al.*, *Phys. Rev. Accel. Beams*, 20:103404, (2017).

[15] J, Qiang, IMPACT-T reference manual, LBNL-62326, (2007).

[16] A. Halavanau, MagnetOptimizer `https://github.com/NIUaard/MagnetOptimizer`, (2017).